Using Artificial Demonstrations Emulating Human Movement Variability for a Learning-based Exoskeleton Flow Controller

Aymeric Orhan, Duy Hoàng, Olivier Bruneau, Bastien Berret, Franck Geffard

Using Artificial Demonstrations Emulating Human Movement Variability for a Learning-based Exoskeleton Flow Controller

Aymeric Orhan, Duy Hoàng, Olivier Bruneau, Bastien Berret and Franck Geffard

***Abstract*— Robotic exoskeletons hold great potential for reducing physical effort and mitigating work-related musculoskeletal disorders. Nevertheless, designing exoskeletons that assist users without disrupting their natural movement remains challenging, as these devices must align seamlessly with human motor intent. Human motor control involves intricate interactions among the nervous system, musculoskeletal system, and environment, leading to movements that are inherently variable. This letter introduces a novel approach using a stochastic optimal control model of human movement to generate synthetic demonstrations preserving this variability, facilitating training by eliminating the need for real user demonstrations. Using a learning-based method, the human motion is predicted in real-time, enabling an adaptive flow controller to dynamically modulate assistance. Specifically, we increase assistance during periods of high variability, when users should tolerate deviations. Experiments with the ABLE7D upper-limb exoskeleton during reaching movements demonstrated that this approach effectively increases interaction comfort, and matches the performance of methods trained on numerous real demonstrations. Furthermore, our findings indicate that non-personalized synthetic demonstrations do not compromise user comfort, supporting the feasibility of a plug-and-play exoskeleton experience.**

I. Introduction

Exoskeletons have proven to be a promising innovation for enhancing human movement, delivering notable advantages in various fields, including rehabilitation and medical applications [1], workplace ergonomics, and augmented physical performance [2]. By focusing on specific joints or muscle groups, these devices can alleviate the physical strain, lower the risk of musculoskeletal disorders, and boost user endurance [3]. Despite these benefits, achieving a seamless human-exoskeleton interaction remains a critical challenge. For an exoskeleton to be truly effective, it must provide assistance in a way that feels natural and unobtrusive to the human user [4].

This work has been submitted to the IEEE (RA-L) for possible publication. Copyright may be transferred without notice, after which this version may no longer be accessible.

Duy Hoàng is with the Université de Versailles Saint-Quentin-en-Yvelines, Université Paris-Saclay, 78035 Versailles, France.

Aymeric Orhan and Olivier Bruneau are with the LURPA, Mechanical Engineering Department, ENS Paris-Saclay, Université Paris-Saclay, 91190 Gif-sur-Yvette, France.

Bastien Berret is with the CIAMS,Université Paris-Saclay, Inria, 91190 Gif-sur-Yvette, France.

Franck Geffard, Aymeric Orhan and Duy Hoàng are with the Université Paris-Saclay, CEA, List, F-91120, Palaiseau, France

This work is supported in part by the French National Agency for Research (grant ANR-19-CE33-0009)

Correspondence should be adressed to Aymeric Orhan: orhanaymeric@gmail.com

Classical strategies to address this challenge consist of leveraging physiological recordings from users to predict their motion intent. Methods such as electroencephalography (EEG) [5], electromyography (EMG) [6], and gaze tracking [7] have enabled the detection of human motion intent at a high level. However, these methods typically identify only broad intents, such as the movement direction or its target location, which are insufficient for fine-tuning exoskeleton assistance throughout an entire motion. In cases where the forthcoming trajectory is not predefined, prediction is often based on regression using continuous EMG signals [8] or kinematic data, as commonly employed in learning-by-demonstration (LBD) approaches [9]. However, these methods often require a large amount of movement demonstrations for their practical implementation.

Recently, a hybrid method has been proposed that integrates state-of-the-art human motor control models, specifically stochastic optimal feedforward-feedback control theory [10], to supply probabilistic movement primitives (ProMPs) [11], a LBD approach, with artificial demonstrations generated offline [12]. This method enables accurate and rapid online trajectory predictions without requiring an extensive training phase, enhancing the system's usability for real-world applications where collecting numerous subject-specific data is impractical. However, this hybrid method had not been tested on a real robotic system.

In this paper, we evaluate the performance of a classical LBD assistive control scheme when using artificial versus real movement demonstrations as the training dataset. More precisely, we employ the Flow Controller (FC) from [13], [14], which establishes a flow field around a reference trajectory predicted by the LBD framework. Using robotic assistance based on a reference trajectory is a well-established approach in many exoskeleton control strategies [15]. The FC approach introduced by [13] applies corrective torques analogous to viscous forces along the flow field surrounding the reference trajectory. This method has demonstrated effectiveness in guiding users while being less resistant to deviations than earlier methods [16], as shown in applications with lower-limb exoskeletons. The work of [14] extended the method to upper-limb exoskeletons, showing that dynamically updating the reference trajectory can significantly enhance the assistance. Here, our contribution is twofold. First, we replace real demonstrations by artificial ones to learn the ProMPs. To preserve the natural variability of human movement, we employ a stochastic optimal control model [10]. Similar to [14], those demonstrations are used to provide continuous online predictions. Additionally, we adjust the FC

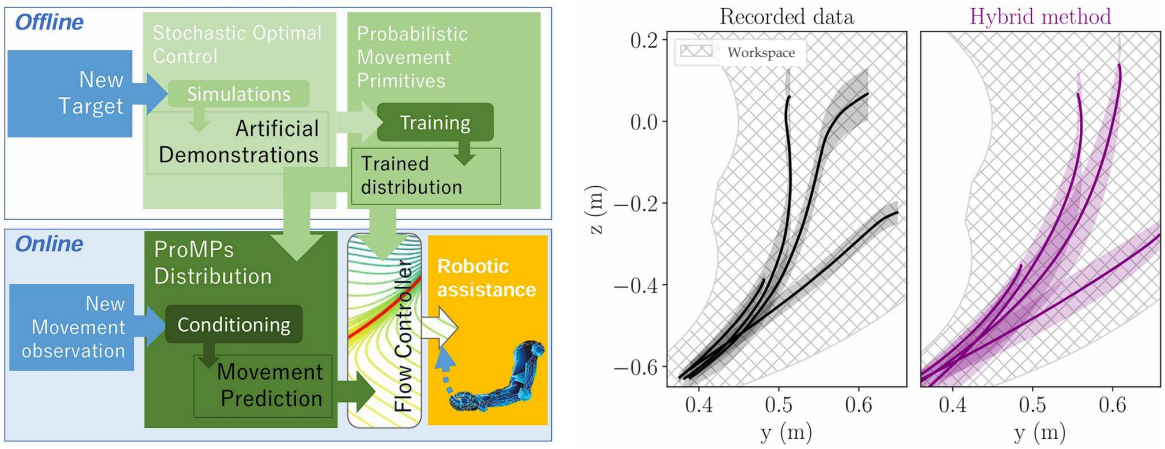

Fig. 1. Left panel: Global overview of the methodology. Right panel: comparison of recorded experimental trajectories and artificially-generated trajectories for the targets in our experiment (mean and std in plain line and shaded area respectively). A notable difference at the end of the movement can be observed, where participants have a terminal approach strategy to the targets that is not reproduced by the stochastic optimal control model of our hybrid method. We accommodate this discrepancy in the control strategy by providing a more compliant assistance at the end of the movement.

parameters to leverage knowledge about human movement variability. Instead of viewing this variability as an obstacle, we utilize variability information derived from stochastic optimal control and ProMPs to modulate the flow field characteristics and the assistive force. In summary, our hybrid approach introduces a variability-informed, demonstration-free version of previous LBD assistive schemes based on FCs.

To test our approach, we conducted an experimental study involving a reaching task with 11 participants. We compared the performance of the original FC design from [14] —utilizing target- and user-specific experimental data (denoted as ODFC, Original Data FC)— and a version using artificially generated data based on our hybrid method (denoted as OHFC, Original Hybrid FC). Additionally, we tested the variability-informed extension of the FC for both scenarios, referred to as IDFC (Improved Data FC) and IHFC (Improved Hybrid FC), respectively. We collected motion-related data, including EMG measurements of the elbow and shoulder flexor and extensor muscles, alongside qualitative feedback from participants.

Results showed that the controllers based on data trained with artificial trajectory demonstrations matched the performance of those trained with 15 real demonstrations per target, without compromising the quality or comfort of assistance. Furthermore, incorporating information about human movement variability in the FC improved user comfort and assistance. These findings suggest that such a control scheme free of real demonstrations but efficiently leveraging the variability of human movement, can offer an effective plug-and-play solution to assist users during repetitive reaching movements.

II. Materials and Methods

A. Trajectory prediction

Reference trajectories for the FC are derived using ProMPs, a LBD approach that predicts future motions based on prior trajectory demonstrations from either the user or a model. In this study, we extend our previous work presented in [12] to synthesize artificial trajectories and assess their influence on the quality of human-exoskeleton interaction in comparison to real trajectory demonstrations. This sections introduces the framework for artificial data generation. An outline of the overall method can be found in Fig. 1.

Artificial Trajectory Generation. Artificial data are generated using a model of human motor control, namely the stochastic optimal feedforward-feedback control model [10]. This method aims at replicating the mean human trajectories and their variability in reaching tasks. The mean trajectories result from an optimal feedforward control minimizing a composite cost function incorporating energy expenditure, joint acceleration, and a cost of time [17], [18]. The variance of trajectories is simulated by considering the effects of sensorimotor noise (modeled as Gaussian processes). To this aim, a locally-optimal feedback control minimizing task-related errors and corrective effort is used. In this task, the human arm is modeled as a two-joint rigid body with shoulder and elbow flexion/extension angles q_1 and q_2. The upper-arm and forearm have lengths, masses, and inertia (l_1, m_1, I_1) and (l_2, m_2, I_2), with total length $L = l_1 + l_2$. Using Lagrangian mechanics, the arm dynamics are classically modeled as:

$$\boldsymbol{\tau} = \mathcal{M}(\boldsymbol{q})\ddot{\boldsymbol{q}} + \mathcal{C}(\boldsymbol{q}, \dot{\boldsymbol{q}})\dot{\boldsymbol{q}} + \mathcal{G}(\boldsymbol{q}) + \mathcal{F}\dot{\boldsymbol{q}}, \tag{1}$$

where $\boldsymbol{\tau} = (\tau_1, \tau_2)$ and $\boldsymbol{q} = (q_1, q_2)$ are the torque and joint angle vectors. $\mathcal{M}, \mathcal{C}, \mathcal{G}$, and $\mathcal{F}$ represent the inertia matrix, Coriolis/centripetal matrix, gravitational vector, and damping matrix, respectively. Furthermore, a smooth torque production is ensured by modeling torque as a twice-differentiable

function of time [17] by setting the motor command $\boldsymbol{u}$ as:

$$\dddot{\boldsymbol{\tau}} = \boldsymbol{u}. \tag{2}$$

Afterwards, the dynamics were discretized using the explicit Euler's scheme.

Deterministic Feedforward Optimal Control. The mean trajectories are generated by solving a discrete-time optimal control (OC) problems that minimize the cost function C_{ff} described by Eq. 3 under dynamical constraints given by Eqs. 1-2 [17]:

$$C_{\text{ff}} = \sum_{t=0}^{T-1} \alpha_1 \ddot{\boldsymbol{q}}_t^\top \ddot{\boldsymbol{q}}_t + \alpha_2 \left(|\dot{q}_{1,t}\tau_{1,t}| + |\dot{q}_{2,t}\tau_{2,t}|\right) + \frac{\alpha_3}{1+\zeta t} \tag{3}$$

where ζ is a cost-of-time parameter taken from [18] (ζ=4.3) and T is the number of time steps. This cost function combines energy expenditure, joint acceleration and time objectives, weighted by factors $(\alpha_i)_{i\in\{1,2,3\}}$ derived from prior studies [12], without subject-specific adjustments. Hard constraints for the initial and final states (at timestep T) were considered as well as state/control constraints for biological plausibility (see supplementary material of [17]). The system's state is defined as $\boldsymbol{x} = (\boldsymbol{q}, \dot{\boldsymbol{q}}, \boldsymbol{\tau}, \dot{\boldsymbol{\tau}})$.

The discrete-time control problem is converted into a non-linear programming problem and solved using the CasADI software [19] with the IPOPT solver [20]. At this stage, we obtain $(\bar{\boldsymbol{u}}, \bar{\boldsymbol{x}})$, the mean state trajectory and control for each reaching movement. The generated trajectories serve as motion plans, around which human variability is modeled using a linear-quadratic-Gaussian (LQG) approach [10], [21].

Stochastic Locally-Optimal Feedback Control. To incorporate variability and generate human-like trajectories, noise in motor commands and sensory feedback are modeled as Gaussian disturbances. Locally-optimal feedback control, effective in the vicinity of the nominal trajectory, corrects task-relevant deviations as described below.

We assume that the sensorimotor system follows the following stochastic difference equation:

$$\begin{aligned} \boldsymbol{x}_{t+1} &= \boldsymbol{f}(\boldsymbol{x}_t, \boldsymbol{u}_t) + \boldsymbol{G}(\boldsymbol{u}_t)\boldsymbol{\xi}_t \\ \boldsymbol{y}_t &= \boldsymbol{g}(\boldsymbol{x}_t) + \boldsymbol{\eta}_t \end{aligned} \tag{4}$$

where $\boldsymbol{x}_t$ is the stochastic state, $\boldsymbol{f}$ is the deterministic dynamics of Eqs. 1-2, and $\boldsymbol{G}$ models the dynamical effects of motor noise. The sensory feedback $\boldsymbol{y}_t$ is given by the output function $\boldsymbol{g}$ that defines how the actual state is observed and will be defined later. The noise terms $\boldsymbol{\xi}_t$ and $\boldsymbol{\eta}_t$ are i.i.d. zero-mean Gaussian variables representing motor and observation noise, respectively.

The matrix $\boldsymbol{G}$ captures both additive and multiplicative noise in the motor command. Thus, we assume that the motor noise acts at the control level $\boldsymbol{u}$, with additive components $\boldsymbol{\sigma} = (\sigma_1, \sigma_2)$ and multiplicative components $\boldsymbol{\lambda} = (\lambda_1, \lambda_2)$, for the elbow and shoulder respectively.

Assuming feedback control keeps the system near the planned trajectory, we linearized it around $(\bar{\boldsymbol{u}}, \bar{\boldsymbol{x}})$ to formulate the LQG problem.

By defining

$$\begin{aligned} &\delta\boldsymbol{x}_t = \boldsymbol{x}_t - \bar{\boldsymbol{x}}_t \quad , \quad \delta\boldsymbol{u}_t = \boldsymbol{u}_t - \bar{\boldsymbol{u}}_t \\ &\boldsymbol{A}_t = \frac{\partial \boldsymbol{f}}{\partial \boldsymbol{x}}_{|\bar{\boldsymbol{x}}_t, \bar{\boldsymbol{u}}_t}, \quad \boldsymbol{B}_t = \frac{\partial \boldsymbol{f}}{\partial \boldsymbol{u}}_{|\bar{\boldsymbol{x}}_t, \bar{\boldsymbol{u}}_t} \text{ and } \quad \boldsymbol{C}_t = \frac{\partial \boldsymbol{g}}{\partial \boldsymbol{x}}_{|\bar{\boldsymbol{x}}_t} \end{aligned} \tag{5}$$

and setting $\boldsymbol{G}_t = \boldsymbol{G}(\bar{\boldsymbol{u}}_t)$, the linearized system becomes:

$$\begin{aligned} \delta\boldsymbol{x}_{t+1} &= \boldsymbol{A}_t\delta\boldsymbol{x}_t + \boldsymbol{B}_t\delta\boldsymbol{u}_t + \boldsymbol{G}_t\boldsymbol{\xi}_t \\ \delta\boldsymbol{y}_t &= \boldsymbol{C}_t\delta\boldsymbol{x}_t + \boldsymbol{\eta}_t \end{aligned} \tag{6}$$

Together with a quadratic cost C_{fb}, this forms a tractable LQG problem for computing the locally-optimal feedback control that corrects task-relevant errors (i.e. deviations that threaten task success). The feedback cost function is defined as:

$$C_{\text{fb}}(\delta\boldsymbol{u}_{0:T}) = \mathbb{E}\left[\delta\boldsymbol{x}_T^\top \boldsymbol{Q}\, \delta\boldsymbol{x}_T + \sum_{t=0}^{T-1} \delta\boldsymbol{u}_t^\top \delta\boldsymbol{u}_t\right] \tag{7}$$

where $\boldsymbol{Q} = \rho\,\text{diag}(1,1,0,0,0,0)$ as in [10], penalizing only the final arm posture. The parameter ρ controls final accuracy, influencing the optimal feedback gain $\boldsymbol{K}_t$ which is such that $\delta\boldsymbol{u}_t = -\boldsymbol{K}_t\delta\widehat{\boldsymbol{x}}_t$ with $\delta\widehat{\boldsymbol{x}}_t$ the optimal state estimate [21]. Since C_{fb} minimizes effort and reach errors, corrections adhere to the minimum intervention principle [22].

For the state estimation, we assume that we observe the full state (i.e., joint positions, velocities, torques, and torque changes) as in [10], setting $\boldsymbol{g}(\boldsymbol{x}) = \boldsymbol{x}$ so that $\boldsymbol{C}_t = \boldsymbol{I}$. The optimal state estimate $\hat{\boldsymbol{x}}_t$ is obtained via a Kalman filter with gain $\boldsymbol{L}_t$. The LQG solution can be found in standard textbooks and in [21].

The resulting variability pattern of this model captures the natural variability of human movement trajectories, enhancing the biomimicry of the artificial demonstrations at both the average behavior and trial-to-trial variation levels. For illustration purposes, recorded and generated data for our experimental task are shown in Fig. 1.

ProMP Encoding and Prediction. ProMPs [11] are employed to encode both demonstrated and artificial trajectories into a probabilistic framework. The trajectories are represented as weight vectors associated with Gaussian basis functions in the task space. Observations of partial movements are used to condition the learned distribution, enabling real-time prediction of the remaining trajectory. The prediction is updated continuously at 20 Hz during the assistive task, ensuring responsiveness to user movements as in [14].

B. Adaptive Flow Controller

Our controller design is derived from the FC presented in [13], [14]. This controller defines the assistance from a flow field that is shaped from a reference trajectory. We used the same formulation as in [13], [14], but used variability information to dynamically adjust the flow controller during the movement execution, as proposed/described below.

Let us denote the current position in the cartesian space as $\mathbf{p}_{c,t} = (y_t, z_t)$ at timestep $t \in \{0, 1, ..., T\}$ during a trajectory. The reference trajectory is obtained using the ProMPs

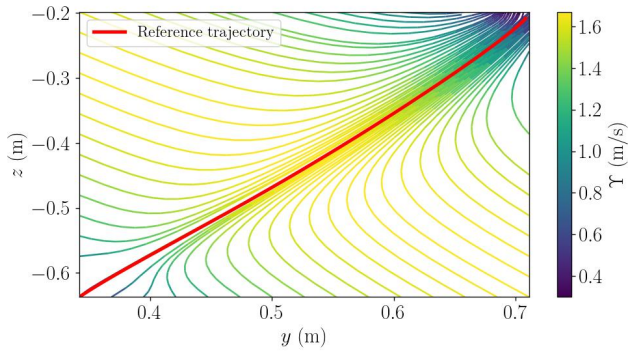

Fig. 2. Flow field representation for target 2 (T_2) illustrates our proposed improvement. The controller's compliance is particularly evident in the early and late phases of the movement. This dynamic compliance results from the field being continuously adjusted during assistance, driven by updates to the reference trajectory using the predictions.

prediction. The reference position $\mathbf{p}_{ref,t}$ corresponding to $\mathbf{p}_{c,t}$ is then defined as the closest point to the current position, in the Cartesian space of the reference trajectory. The corresponding phase is thus taken as the current phase (the normalized time, denoted by τ) of the movement. For this section, we alleviate the notation and omit the time/phase dependence. The Cartesian error vector is then defined with $\mathbf{e} = \mathbf{p}_{ref} - \mathbf{p}_c$.

The normalized tangent $\mathbf{t}$ and normal $\mathbf{n}$ vectors at point $\mathbf{p}_{ref}$ of the current ProMP distribution, are respectively denoted by $\mathbf{t}$ and $\mathbf{n}$. This tangent vector and $\mathbf{n}$, the normal vector to the reference trajectory at $\mathbf{p}_{ref}$, are used to define another normal vector $\hat{\mathbf{n}}$ that, when placed at $\mathbf{p}_c$, points towards the reference trajectory:

$$\hat{\mathbf{n}} = \begin{cases} -\mathbf{n} & \text{if } \theta < 90° \\ \mathbf{n} & \text{else} \end{cases} \tag{8}$$

where θ is the angle between $\mathbf{e}$ and the normal to the curve.

The equation of the flow field is then defined by the field's velocity $\mathbf{v}_{ref}$ as a compromise between a tangential and normal component, i.e. an assistive and a corrective component using these vectors:

$$\mathbf{v}_{ref} = \begin{cases} \Upsilon \frac{(|e|\hat{\mathbf{n}} + \frac{K_{sh}}{|e|}\mathbf{t})}{|(|e|\hat{\mathbf{n}} + \frac{K_{sh}}{|e|}\mathbf{t})|} & \text{for } |e| \geq 1e^{-5} \\ \Upsilon \mathbf{t} & \text{for } |e| < 1e^{-5} \end{cases} \tag{9}$$

where Υ and K_{sh} are two scalars defining respectively the magnitude of the velocity and the compromise between the assistive and corrective repartition of the assistance along the tangential and normal vector previously defined. The threshold for $|e|$ is set as in [14].

We dynamically modify the parameters Υ and K_{sh} of the FC along the phase of the movement according to velocity profiles and human variability information obtained from demonstrations (either experimental or artificial).

The parameter K_{sh} is inversely proportional to the correctiveness of the controller. When K_{sh} is high, the assistance is slightly corrective whereas if K_{sh} is low, the assistance is highly corrective. We also posit that when variability is high we can increase the correctiveness of our assistance as the user will be more likely to accept deviations from the trajectory.

More precisely, we define K_{sh} using two empirical constants. These values, M_{var} and m_{var} correspond respectively to the maximum and the minimum of standard deviation measured from the demonstrations. Similarly, we denote v as the standard deviation value at the current phase. We then define K_{sh} as a remapping of these values between chosen K_{sh} bounds: $[5e^{-3}, 5e^{-2}]$ (m^2), tuned by hand in during preliminary trials.

$$K_{sh} = 5e^{-3} + \frac{4.5e^{-2}(v - m_{var})}{M_{var} - m_{var}} \tag{10}$$

However this definition can lead to highly corrective assistance at the start and end of the movement which can lead to high resistance for the user if its actual intent and our prediction diverge. To counter this effect we set K_{sh} equal to $8e^{-2}m^2$ when the phase is lower than 0.1 or higher than 0.9. This way 10% of the assistance at the beginning and at the end is hard-coded to ensure a compliant assistance to user intent. Fuzzy logic functions are used to smoothly transition out and in of those regions.

The parameter Υ corresponds directly to the magnitude of the flow field's reference velocity as defined by equation (9). More concretely, Υ defines the exoskeleton's hand target velocity value. In this work, the preferred human velocity is considered at each motion phase rather than the maximum value of velocity to modulate our assistance. Two values are used to define Υ: $\hat{V}_t$ and V_t^M, respectively the mean and maximum velocity observed at the current timestep of the movement in the demonstrations. Υ is then defined at the timestep t with the following equation:

$$\Upsilon_t = \hat{V}_t + \frac{1}{T+1}\sum_{k=0}^{T}(V_k^M - \hat{V}_k) \tag{11}$$

The first component of the equation (11) mimics the mean behavior of the user while the second component ensures the assistive capacity of the robot since the reference velocity is always greater than the human velocity.

Once the flow field is defined, the assistive force of the exoskeleton is set as a force due to drag applied by a viscous fluid on an immersed symmetric body:

$$\mathbf{F}_a = C_{drag}(\mathbf{v}_{ref} - \mathbf{v}_c) \tag{12}$$

where $\mathbf{v}_c$ is the current hand velocity vector, estimated with the exoskeleton's incremental encoders and C_{drag} is the drag coefficient set equal to 20Ns/m as in [14]. The assistive force $\mathbf{F}_a$ was updated at a frequency of 1Khz for all conditions. A representation of the flow field with these definitions of Υ and K_{sh} can be found in Fig. 2.

In the original flow controller formulated in [14], a 250ms waiting period after movement onset is used before activation of the assistance in an attempt to not disturb the movement. Our modulation of Υ and K_{sh} allowed us to eliminate this waiting period in our proposed improvement while still

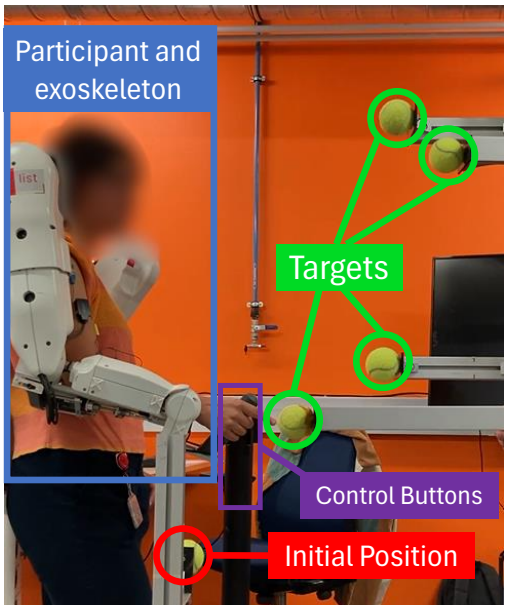

Fig. 3. Experimental setup. Participants started their reaching movements at the initial position to a given target, starting the assistance with the control buttons. Note that T_3 has been slid back in this picture to free the workspace of any visual obstacle for the participant for reaching movements towards T_1.

offering a compliant albeit low assistance in the beginning of the movement.

C. Experimental Design

To evaluate the performance of our dynamic FC we conducted an experiment with 11 participants. In the following section we describe the experimental design and protocol.

Task: The experiment was divided in 5 blocks. During the first block participants were asked to perform 15 reaching movements towards targets in front of them as shown in Fig. 3. The demonstrations obtained were then used to train ProMPs distribution for each target and used for predicting upcoming movements with the ODFC and IDFC as explained in II.A. The 4 other blocks were conducted in a random order for each participant. They consisted of performing the same reaching movements with the ODFC, OHFC, IDFC or IHFC. After each of these 4 blocks we collected the participants qualitative results using a survey, described in III.A, and a NASA-TLX questionnaire. Participants remained unaware of the nature and of which assistive mode they were evaluating until the experiment was completely finished.

Participants: Eleven healthy young adults (3 Females) participated in the experiment. The participants, with a mean age of 29.91 ± 2.39 years, mean height of 1.75 ± 0.1m, and mean weight of 67.09 ± 12.27kg, were right-handed adults without any known neurological disorders or injuries that could have affected the experiment. Written informed consent was obtained from all participants in accordance with the Helsinki declaration, and the protocol was approved by the local ethical committee for research.

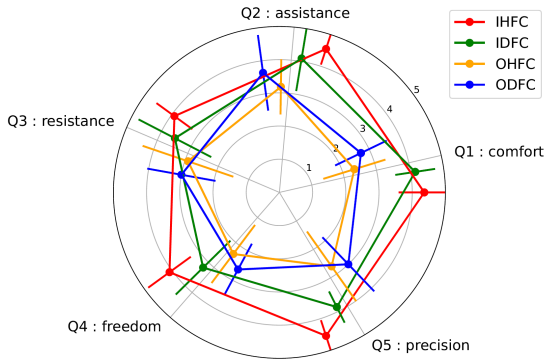

Fig. 4. Qualitative results to the questionnaire (mean+std for each question).

Data Collection: The reaching task was performed while wearing a backdrivable robotic exoskeleton for the upper limb (ABLE, [23]). This exoskeleton features seven active joints, three replicating the human gleno-humeral joint, one emulating human elbow flexion/extension and three recreating the radiocarpal joint. Movements were measured using the internal encoders of the exoskeleton worn by participants at a frequency of 1 kHz. We measured the EMG signals of 6 muscles responsible for shoulder and elbow flexion and extension: the posterior and anterior deltoids, the lateral and long-head triceps, the biceps and the brachioradialis. The EMG sensors were placed according to the SENIAM recommendations [24].

III. Results

A. Qualitative Results

Participants' subjective feedback on each assistive mode was assessed using a 5-point Likert scale, ranging from strongly disagree (0) to strongly agree (5). Five statements were evaluated by the participants:

- Q1: Achieving the task was comfortable.
- Q2: The robot assisted me in accomplishing the task.
- Q3: The robot did not resist my movement.
- Q4: I felt free to execute my movement as I wanted to.
- Q5: I could accurately reach the target.

As stated in section II.C we additionally estimated the physical exertion of participants after each experimental block using a NASA TLX questionnaire. To limit desirability bias [25], participants were asked to give an immediate answer and that there was no right or wrong answer, they could also give us written or additional remarks. Furthermore, the experiment occurred in full anonymity. This questionnaire has already been used in the field exoskeleton upper-limb assistance [26] and as such allows comparisons with other control mode in the literature. We go into further detail in the analysis of this questionnaire's results than the NASA TLX questionnaire as it is more relevant to our field of study and provides a clearer idea of the participant's feedback.

Results to the Likert-scale questionnaire are shown in Fig. 4. A statistical analysis was conducted and statistical

significance ($p < 0.05$). A Shapiro-Wilk test was first realized and revealed that the data distribution was not normal after which we conducted a Wilcoxon-Nemenyi test on each question for each assistive mode to assess significance. A statistical significance was established for questions 4 and 5 ($p = 0.0260$ and $p = 0.0235$) between the IHFC and IDFC. Statistical significance between improved and original control mode was established for all questions. No statistical significance was established on any question between the OHFC and ODFC conditions.

Similarly we conducted a statistical with the same procedure for the NASA TLX weighted ratings results. We established statistical significance between improved (IHFC: 27.76 ± 14.90 and IDFC: 33.18 ± 16.11) and original (OHFC: 49.73 ± 15.59 and ODFC: 52.82 ± 14.45) controller modes. No statistical significance was found between IHFC and IDFC, nor between OHFC and ODFC.

Generally participants expressed a strong preference for our proposed enhanced mode. Although the results show no difference between OHFC and ODFC, participants expressed a preference for the ODFC mode. Interestingly, a majority also expressed a preference for the IHFC condition over the IDFC condition and also overall. We believe that this is due to the size of the artificial datasets (1000 trajectories) that produces higher variability than the experimental ones (15 to 20 movements), making for a stronger (a fast movement systematically exists in the dataset) and more adaptive (due to increased variability) assistance with our design. One could also argue that demonstrated movements in transparent mode tend to be slowed down from actual natural movements as studied in [26], which led to a weaker assistance with our design due to the definition of Υ.

B. Quantitative Results

Impact on movement kinematics. A significant alteration in movement kinematics was observed, as illustrated in Fig. 5 and Fig. 7. This outcome is expected, as the target speed of the assistance is considerably higher than the participants' average natural movement speed, due to the definition of the Υ parameter in the FC design. Consequently, the duration of movements, shown in Fig. 6, was also affected, with a statistically significant difference noted between the transparent mode and the four assistive modes. Additionally, the RMS of the assistive force from the exoskeleton for each control mode is presented in Fig. 6.

Impact on muscle activation and co-contraction. The difference of movement duration and speed between the transparent and assistive modes makes the comparison of muscle activation with EMG signals hard to compare as shown in [27], [28]. However, they can be used to compare the impact of each assistive mode on muscle activations as movement duration and speed variations across these are not statistically significant (according to a Friedman and subsequent Wilcoxon-Nemenyi test). We show in Fig. 8 the muscle activation results for the assistive modes.

Statistical analysis was performed to identify significant differences between control conditions. A significant main

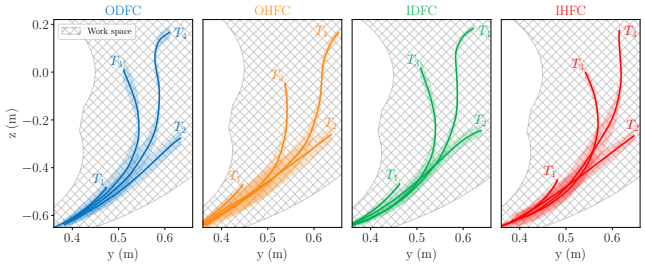

Fig. 5. Cartesian movements for each target and assistive condition, across all participants (mean and std in plain line and shaded area respectively). The impact of the used demonstrations shown in fig 1 is clearly visible.

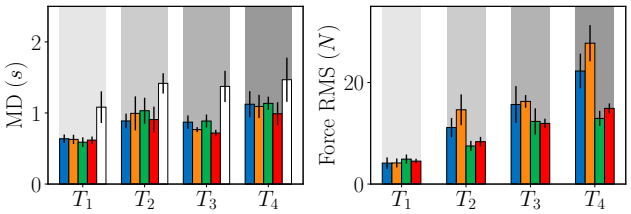

Fig. 6. Left panel : Movement duration. Right Panel : Assistive force. Both metrics for all assistive conditions and transparent mode as well for movement duration, for the four targets across all participants. Legend is identical as Fig. 7.

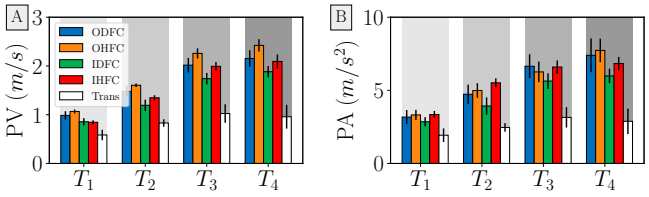

Fig. 7. Peak velocity (panel A) and peak acceleration (panel B) for all assistive condition and transparent mode. Note a clear augmentation for all assistive mode compared to the transparent mode.

effect was observed for elbow flexors ($Q = 48.41, ; p = 7.10^{-10}$) and elbow extensors ($Q = 36.29, ; p = 3.10^{-7}$). For elbow flexors, ODFC and OHFC elicited significantly higher muscle activity compared to IDFC and IHFC ($p < 0.006$). However, no significant difference was found between ODFC and OHFC, or between IDFC and IHFC.

We computed a co-contraction index as defined in [29]. The results for this index for the elbow and shoulder across all participants and assistive mode is shown in Fig. 9. We conducted a statistical analysis that established a significant reduction of muscle co-contraction for both joints between the original and improved FC. No significant difference was found between hybrid and experimental data trained assistive modes. We observed a statistically significant increase between the transparent mode and the assistive mode for the shoulder but not for the elbow.

C. Discussion

What is the impact of using artificially generated data? Quantitative results showed no difference between training

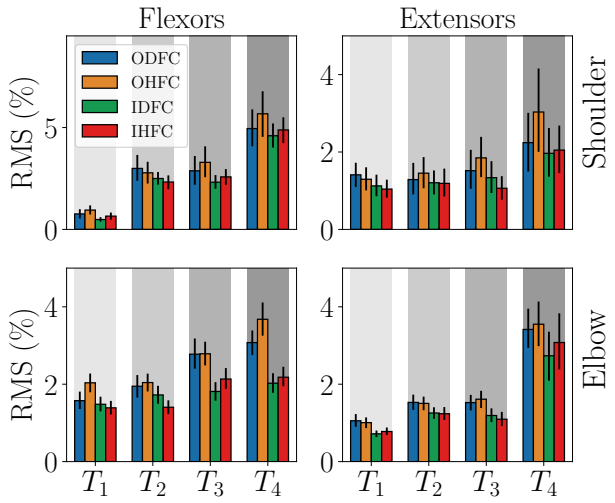

Fig. 8. Measured muscle activation for the shoulder and elbow flexor and extensor muscles across all participants.

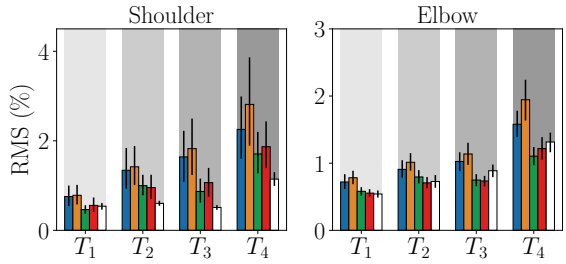

Fig. 9. Measured co-contraction of the shoulder and elbow muscles for all assistive condition and transparent mode across all participants. Legend is identical as Fig. 7.

the ProMPs prediction method with experimental or artificial data. However, we reported a better performance for the artificially trained FC in the qualitative analyses regarding the feeling of freedom and accuracy, and no difference in the rest of the items. Nevertheless, the artificial data generation is limited by the necessity of tailoring the cost function to the task at hand. The present task was previously investigated in [17] so a good knowledge of a plausible cost function was available. Although inverse optimal control (as in [17]) can be used for this purpose, this would require real movement demonstrations. In the future, it would be interesting to test our method with subject-specific cost functions and for a more diverse set of movements, but the present results suggest that a generic cost function could be sufficient to provide an effective and comfortable assistance if the human movement variability is considered.

What is the impact of modulating the assistance according to movement variability? We demonstrated that modulating the assistance based on human movement variability significantly improved the FC. Stronger corrective assistance was applied in regions of high variability, leading to smoother interactions and minimizing the exoskeleton's resistance by accommodating better user habits. While the assistive force (see Fig. 6) is lower with this approach, it helps mitigate adverse effects, such as increased user stiffness. Evidence of reduced muscle activation (Fig. 8) and co-contraction (Fig. 9) supports this conclusion. Our variability-informed design thus offers a more comfortable interaction than classical methods but still requires comparison with approaches. Interestingly, the present trajectory prediction could be combined with more advanced control schemes such as those based on differential game theory [30].

IV. Conclusion

Recent approaches in upper-limb exoskeleton control have focused on designing non-invasive approaches relying on prediction of human motion intent [4]. Although the absence of bio-information inevitably limits movement prediction capabilities, efficient and comfortable assistance have still been successfully achieved, especially in repetitive tasks when human movement demonstrations are available [13], [14], [16].

Some techniques integrate human movement variability [14], [31], which can enhance human-robot interaction [14]. Here, we leveraged this information to modulate upper-limb exoskeleton assistance via an adaptive flow controller. Our results suggest that considering movement variability improves interaction, reducing the adversarial effects of robotic assistance, as shown by decreased muscle co-contraction.

However, these types of approaches are still constraining in many regards, mainly due to their lack of generality and the necessary training period. Whereas these drawbacks might be acceptable in rehabilitation settings, they constitute important limits for an actual use in an industrial setting. Here, we have proposed a hybrid approach to replace real user demonstrations by stochastic optimal control simulations retaining the human variability that is crucial to learning-by-demonstration methods, which themselves provide online usability.

Further work could extend our approach to situations where the controller is not informed about which particular target the user wants to reach, so as to increase the usability and generality of our approach. In such cases, one could use classification strategies that have been recently developed using ProMPs [31] to infer the user's goal and associated trajectory.

Overall, our approach could enhance the interaction between the exoskeleton and the user without requiring real demonstrations, providing seamless and efficient assistance. This could facilitate the practical use of assistive exoskeletons in demanding industrial environments by eliminating the need for time-consuming training periods.

References

[1] T. Proietti, V. Crocher, A. Roby-Brami, and N. Jarrasse, "Upper-Limb Robotic Exoskeletons for Neurorehabilitation: A Review on Control Strategies," *IEEE reviews in biomedical engineering*, 2016. DOI: 10.1109/RBME.2016.2552201.

[2] M. A. Nussbaum, B. D. Lowe, M. de Looze, C. Harris-Adamson, and M. Smets, "An Introduction to the Special Issue on Occupational Exoskeletons," *IISE Transactions on Occupational Ergonomics and Human Factors*, no. 3-4, 2019. DOI: 10.1080/24725838.2019.1709695.

[3] G. Bao, L. Pan, H. Fang, *et al.*, "Academic Review and Perspectives on Robotic Exoskeletons," *IEEE transactions on neural systems and rehabilitation engineering: a publication of the IEEE Engineering in Medicine and Biology Society*, no. 11, 2019. DOI: 10.1109/TNSRE.2019.2944655.

[4] Y. Li, A. Sena, Z. Wang, *et al.*, "A review on interaction control for contact robots through intent detection," *Progress in Biomedical Engineering*, 2022. DOI: 10.1088/2516-1091/ac8193.

[5] C. Huang, Y. Xiao, and G. Xu, "Predicting Human Intention-Behavior Through EEG Signal Analysis Using Multi-Scale CNN," *IEEE/ACM transactions on computational biology and bioinformatics*, no. 5, 2021. DOI: 10.1109/TCBB.2020.3039834.

[6] E. Trigili, L. Grazi, S. Crea, *et al.*, "Detection of movement onset using EMG signals for upper-limb exoskeletons in reaching tasks," *Journal of NeuroEngineering and Rehabilitation*, no. 1, 2019. DOI: 10.1186/s12984-019-0512-1.

[7] H. Admoni and S. Srinivasa, "Predicting User Intent Through Eye Gaze for Shared Autonomy," in *AAAI Fall Symposia*, 2016.

[8] K. Kiguchi and Y. Hayashi, "An emg-based control for an upper-limb power-assist exoskeleton robot," *IEEE Transactions on Systems, Man, and Cybernetics, Part B (Cybernetics)*, no. 4, 2012.

[9] S. Calinon, F. D'halluin, E. L. Sauser, D. G. Caldwell, and A. G. Billard, "Learning and Reproduction of Gestures by Imitation," *IEEE Robotics & Automation Magazine*, no. 2, 2010. DOI: 10.1109/MRA.2010.936947.

[10] B. Berret, A. Conessa, N. Schweighofer, and E. Burdet, "Stochastic optimal feedforward-feedback control determines timing and variability of arm movements with or without vision," *PLOS Computational Biology*, no. 6, 2021. DOI: 10.1371/journal.pcbi.1009047.

[11] A. Paraschos, C. Daniel, J. R. Peters, and G. Neumann, "Probabilistic movement primitives," in *Advances in Neural Information Processing Systems*, C. Burges, L. Bottou, M. Welling, Z. Ghahramani, and K. Weinberger, Eds., Curran Associates, Inc., 2013.

[12] A. Orhan, D. Verdel, O. Bruneau, F. Geffard, and B. Berret, "Combining Model-based and Data-based approaches for online predictions of human trajectories," in *IEEE RAS EMBS 10th International Conference on Biomedical Robotics and Biomechatronics (BioRob 2024)*, Heidelberg (Germany), 2024.

[13] A. Martinez, B. Lawson, C. Durrough, and M. Goldfarb, "A Velocity-Field-Based Controller for Assisting Leg Movement During Walking With a Bilateral Hip and Knee Lower Limb Exoskeleton," *IEEE Transactions on Robotics*, no. 2, 2019. DOI: 10.1109/TRO.2018.2883819.

[14] M. Jamšek, T. Kunavar, U. Bobek, E. Rueckert, and J. Babič, "Predictive Exoskeleton Control for Arm-Motion Augmentation Based on Probabilistic Movement Primitives Combined With a Flow Controller," *IEEE Robotics and Automation Letters*, no. 3, 2021. DOI: 10.1109/LRA.2021.3068892.

[15] R. Cao, L. Cheng, C. Yang, and Z. Dong, "Iterative assist-as-needed control with interaction factor for rehabilitation robots," *Science China Technological Sciences*, no. 4, 2021. DOI: 10.1007/s11431-020-1671-6.

[16] A. Duschau-Wicke, J. von Zitzewitz, A. Caprez, L. Lunenburger, and R. Riener, "Path control: A method for patient-cooperative robot-aided gait rehabilitation," *IEEE transactions on neural systems and rehabilitation engineering: a publication of the IEEE Engineering in Medicine and Biology Society*, no. 1, 2010. DOI: 10.1109/TNSRE.2009.2033061.

[17] B. Berret, E. Chiovetto, F. Nori, and T. Pozzo, "Evidence for Composite Cost Functions in Arm Movement Planning: An Inverse Optimal Control Approach," *PLoS Computational Biology*, no. 10, J. Diedrichsen, Ed., 2011. DOI: 10.1371/journal.pcbi.1002183.

[18] B. Berret and F. Jean, "Why Don't We Move Slower? The Value of Time in the Neural Control of Action," *The Journal of Neuroscience: The Official Journal of the Society for Neuroscience*, no. 4, 2016. DOI: 10.1523/JNEUROSCI.1921-15.2016.

[19] J. Andersson, J. Gillis, G. Horn, J. Rawlings, and M. Diehl, "CasADi: A software framework for nonlinear optimization and optimal control," *Mathematical Programming Computation*, 2018. DOI: 10.1007/s12532-018-0139-4.

[20] A. Wächter and L. T. Biegler, "On the implementation of an interior-point filter line-search algorithm for large-scale nonlinear programming," *Mathematical Programming*, no. 1, 2006. DOI: 10.1007/s10107-004-0559-y.

[21] E. Todorov, "Stochastic optimal control and estimation methods adapted to the noise characteristics of the sensorimotor system," *Neural Computation*, no. 5, 2005. DOI: 10.1162/0899766053491887.

[22] E. Todorov and M. I. Jordan, "Optimal feedback control as a theory of motor coordination," *Nature Neuroscience*, no. 11, 2002. DOI: 10.1038/nn963.

[23] P. Garrec, J. Friconneau, Y. Measson, and Y. Perrot, "ABLE, an innovative transparent exoskeleton for the upper-limb," in *2008 IEEE/RSJ International Conference on Intelligent Robots and Systems*, Nice: IEEE, 2008, ISBN: 978-1-4244-2057-5 978-1-4244-2058-2. DOI: 10.1109/IROS.2008.4651012.

[24] H. J. Hermens, B. Freriks, R. Merletti, *et al.*, "European Recommendations for Surface ElectroMyoGraphy," 1999.

[25] M. Patten, *Questionnaire Research: A Practical Guide*, 4th ed. New York: Routledge, 2016, ISBN: 978-1-315-26585-8. DOI: 10.4324/9781315265858.

[26] D. Verdel, A. Farr, T. Devienne, N. Vignais, B. Berret, and O. Bruneau, "Human movement modifications induced by different levels of transparency of an active upper limb exoskeleton," *Frontiers in Robotics and AI*, 2024. DOI: 10.3389/frobt.2024.1308958.

[27] S. H. Brown and J. D. Cooke, "Amplitude- and instruction-dependent modulation of movement-related electromyogram activity in humans," *The Journal of Physiology*, 1981. DOI: 10.1113/jphysiol.1981.sp013775.

[28] D. M. Corcos, G. L. Gottlieb, and G. C. Agarwal, "Organizing principles for single-joint movements. II. A speed-sensitive strategy," *Journal of Neurophysiology*, no. 2, 1989. DOI: 10.1152/jn.1989.62.2.358.

[29] G. Li, M. S. Shourijeh, D. Ao, C. Patten, and B. J. Fregly, "How Well Do Commonly Used Co-contraction Indices Approximate Lower Limb Joint Stiffness Trends During Gait for Individuals Post-stroke?" *Frontiers in Bioengineering and Biotechnology*, 2020. DOI: 10.3389/fbioe.2020.588908.

[30] Y. Li, G. Carboni, F. Gonzalez, D. Campolo, and E. Burdet, "Differential game theory for versatile physical human–robot interaction," *Nature Machine Intelligence*, no. 1, 2019.

[31] O. Dermy, A. Paraschos, M. Ewerton, J. Peters, F. Charpillet, and S. Ivaldi, "Prediction of Intention during Interaction with iCub with Probabilistic Movement Primitives," *Frontiers in Robotics and AI*, 2017. DOI: 10.3389/frobt.2017.00045.